ELSEVIER

Contents lists available at ScienceDirect

### Nuclear Medicine and Biology

journal homepage: www.elsevier.com/locate/nucmedbio





# [ $^{18}$ F]FDG-PET provides insights into the liver-brain axis and confirms $SUV_{gluc}$ as a surrogate for $MR_{Glu}$ in a mouse model of liver fibrosis

Thomas Wanek<sup>a</sup>, Mari Teuter<sup>b</sup>, Asha Balakrishnan<sup>c</sup>, Tobias L. Ross<sup>b</sup>, Frank M. Bengel<sup>b</sup>, Michael Ott<sup>c</sup>, Marion Bankstahl<sup>d,e</sup>, Jens P. Bankstahl<sup>b,\*</sup>

- a Preclinical Imaging Lab (PIL), Department of Biomedical Imaging and Image-guided Therapy, Medical University of Vienna, Vienna, Austria
- <sup>b</sup> Department of Nuclear Medicine, Hannover Medical School, Germany
- <sup>c</sup> Department of Gastroenterology, Hepatology, Infectious Diseases and Endocrinology, Hannover Medical School, Germany
- <sup>d</sup> Institute for Laboratory Animal Science and Central Animal Facility, Hannover Medical School, Germany
- <sup>e</sup> Department of Biological Sciences and Pathobiology, Center for Biological Sciences, Pharmacology and Toxicology, University of Veterinary Medicine Vienna, Vienna, Austria

#### ARTICLE INFO

#### Keywords: [<sup>18</sup>F]FDG PET Quantification Preclinical imaging Brain metabolism Liver fibrosis

#### ABSTRACT

*Purpose*: The liver-brain axis regulates metabolic homeostasis, with glucose metabolism playing a key role. Liver dysfunction, such as fibrosis, may impact brain metabolism and consequently, brain function. Positron emission tomography (PET) imaging provides a non-invasive approach to study glucose metabolism in both organs. A recent longitudinal PET/CT study utilizing 2-deoxy-2-[<sup>18</sup>F]-fluoro-p-glucose ([<sup>18</sup>F]FDG) amongst other radio-tracers revealed significant metabolic changes in the liver in a mouse model of liver fibrosis. Here, we retrospectively analyzed those data to quantify potential associated changes in brain glucose metabolism.

*Procedures*: Eleven male C57BL/6N mice underwent repeated PET imaging with [ $^{18}$ F]FDG at baseline, prefibrosis, fibrosis, and remission stages. Cerebral glucose metabolism was assessed using standardized uptake value (SUV), blood glucose-corrected SUV ( $SUV_{gluc}$ ), and kinetic modeling (Patlak and two-tissue compartment models) for calculation of the glucose metabolic rate ( $MR_{Glu}$ ).

Results: Both  $SUV_{gluc}$  and  $MR_{Glu}$  significantly decreased during pre-fibrosis and fibrosis on whole brain level and recovered at remission.  $SUV_{gluc}$  statistical parametric mapping identified multiple brain areas with reduced glucose metabolism, which was confirmed by regional analysis showing progressive reduction in  $SUV_{gluc}$ . Correlation analyses confirmed  $SUV_{gluc}$  as a reliable surrogate for  $MR_{Glu}$ , unlike uncorrected SUV. Liver [ $^{18}F$ ]FDG uptake increased during fibrosis and normalized at remission, mirroring changes in blood glucose concentrations. Conclusions: [ $^{18}F$ ]FDG PET imaging revealed that liver fibrosis alters glucose metabolism in both liver and brain, emphasizing the potential of molecular imaging for future assessment of metabolic interaction between liver and brain. [ $^{18}F$ ]FDG uptake in terms of  $SUV_{gluc}$  strongly correlated with  $MR_{Glu}$  from kinetic modeling, supporting its utility as a valid surrogate parameter to quantify cerebral glucose metabolism in mice.

#### 1. Introduction

The liver-brain axis is a crucial and complex communication network that plays a significant role in maintaining metabolic homeostasis, regulating energy balance and sustaining cognitive function. One of the key elements in this axis is the regulation of glucose metabolism, which is essential for brain function and cognitive performance. Here, the liver serves as a central hub by balancing the uptake and storage of glucose as well as its production and release into the bloodstream to supply central and peripheral organs and tissues. Understanding the liver-brain axis

and its role in glucose metabolism, along with its implications under pathological conditions, is essential for developing therapeutic strategies for metabolic and neurological diseases [1,2].

Liver and brain communicate bidirectionally via various neural, hormonal and metabolic pathways. Consequently, impaired liver function such as hepatic fibrosis has been suggested to affect cognitive functions via those pathways [3,4]. Fibrosis, a major hallmark of impaired liver function, primarily results from repetitive, often toxic or infectious liver injury, which activates hepatic stellate cells to produce extracellular matrix as part of the wound healing process. Initially

<sup>\*</sup> Corresponding author at: Department of Nuclear Medicine, Hannover Medical School, Carl-Neuberg-Straße 1, 30625, Hannover, Germany. E-mail address: Bankstahl.Jens@mh-hannover.de (J.P. Bankstahl).

reversible, fibrosis can progress into end-stage cirrhosis and then to liver cancer, with significant consequences for the affected subjects [5]. Recently, liver fibrosis, even at the subclinical stage without changes in liver enzyme levels, has been identified as an independent risk factor for cognitive impairment in adult patients [6].

Non-invasive biomarkers and imaging approaches to monitor consequences of liver impairment for other organs, such as the brain are therefore highly sought. Molecular imaging, such as positron emission tomography (PET) with the glucose analogue 2-deoxy-2-[<sup>18</sup>F]-fluoro-Dglucose ([<sup>18</sup>F]FDG) provides a non-invasive and quantitative approach to measure glucose utilization in various tissues [7–9]. Moreover, PET is an excellent translational research tool, as protocols established in preclinical studies can be easily applied in clinical imaging and vice versa. [<sup>18</sup>F]FDG PET studies in humans confirmed glucometabolic impairment in brains of patients with end-stage liver disease such as cirrhosis [10]. Still, preclinical PET studies investigating impairment of liver-brain metabolic coupling in disease models are largely lacking.

The availability of high-resolution small-animal PET scanners with a large transaxial field-of-view enables fundamental research into understanding molecular mechanisms and disease progression on a wholebody level in mice. Small-animal PET studies can be designed as longitudinal studies, meaning that the same animal can be measured at multiple time points. This approach minimizes the number of animals required and maximizes the statistical utility of the data. Moreover, dynamic small-animal [18F]FDG PET imaging enables the exact determination of the cerebral glucose consumption via calculation of the metabolic rate of glucose ( $MR_{Glu}$ ) or the net influx rate ( $k_i$ ) by kinetic modeling approaches [11,12]. Dynamic imaging, however, requires time-consuming PET acquisitions (60-90 min). This can be specifically challenging in longitudinal studies, during which repeated, long-lasting periods of anesthesia are required to immobilize the animals during PET acquisition. Alternatively, semi-quantitative parameters such as the blood-glucose corrected standardized uptake value ( $SUV_{gluc}$ ) could serve as surrogate estimates for cerebral  $MR_{Glu}$  [13–16].

Given that PET data of mice are often acquired on a whole-body basis, retrospective analysis becomes feasible, allowing researchers to explore areas that were not initially the primary focus [17,18]. We recently performed a longitudinal, dynamic PET/CT study in a carbon tetrachloride (CCl<sub>4</sub>) induced model of liver fibrosis in mice. Here, we observed significant changes in [ $^{18}$ F]FDG uptake in the liver, along with alterations in blood glucose levels during the progression of liver fibrosis and at remission [19]. As the brain of the investigated mice was always within the field of view in this study, we retrospectively analyzed [ $^{18}$ F]FDG brain uptake in those animals. We hypothesized i) that brain glucometabolism will be impaired in mice with established liver fibrosis and ii) that brain  $SUV_{gluc}$  is a suitable estimate for  $MR_{Glu}$  and can therefore be used as a more practical substitute to visualize and quantify cerebral glucose metabolism in the murine brain.

#### 2. Materials and methods

#### 2.1. Induction of liver fibrosis

All animal experiments were approved by the respective national state authorities (Niedersächsisches Landesamt für Verbraucherschutz und Lebensmittelsicherheit) under approval ID: 21-3743. All study procedures were in full accordance with the European Communities Council Directive of September 22, 2010 (2010/63/EU). All applicable institutional and national guidelines for the care and use of animals were followed. The description of the study procedure is in line with the ARRIVE guidelines 2.0 [20]. The initial sample size required for this study was based on a priori power analysis assuming an effect size of 1.01 and a power of 80 %.

Eleven male C57BL/6N mice (Crl: C57BL/6NCrl; Charles River Laboratories, Sulzfeld, Germany), aged 10 weeks when purchased, were retrospectively analyzed for this study. Animals were group housed in

enriched individually ventilated BCU cages (Allentown, NJ, USA) under SPF conditions in a temperature and humidity-controlled facility (22  $\pm$  1 °C; 50  $\pm$  5 % humidity), had free access to standard laboratory diet (Altromin, Lage, Germany), autoclaved water ad libitum and were kept under a cycle of 14 h of light and 10 h of dark. An acclimatization and handling period of at least two weeks was allowed before the animals were used. No systematic randomization of animal assignment to experimental group was applied, but animals were randomly picked from the transport box of the animal breeder. A priori established exclusion criteria were not met at the start of the study.

For the induction of liver fibrosis (Fig. 1), repeated administrations of  $CCl_4$  into the abdominal cavity were performed as described previously [21,22]. In brief, 20 % (v/v)  $CCl_4$  (corresponding to 797 mg  $CCl_4$ /kg bodyweight) in corn oil (Sigma-Aldrich, Merck, Germany) was injected intraperitoneally (i.p.) into the lower abdomen of the mice twice per week for a period of six weeks. This scheme is known to induce an intermediate level of liver fibrosis throughout the stages of baseline (no fibrosis), an early phase within three weeks of repeated  $CCl_4$  administrations (pre-fibrosis) that progresses during continuation of  $CCl_4$  injections for a total time of six weeks into an intermediate liver fibrosis (fibrosis). Afterwards, a washout period for another three weeks with no  $CCl_4$  administrations results in remission.

#### 2.2. Small animal PET imaging

The experimental timeline of this study is depicted in Fig. 1. Repeated [18F]FDG PET scans were performed in random order on a dedicated small animal PET scanner (Inveon DPET, Siemens Medical Solutions, Knoxville, TN, USA) at baseline, pre-fibrosis, fibrosis and remission stages. Mice were not fasted before PET imaging. For anesthesia induction, single mice were placed in an induction box and anesthetized with isoflurane/oxygen (3.5 % v/v). When unconscious, the animals were positioned on a heated mat while anesthesia was continued. Protective eye ointment (Bepanthen, Bayer AG, Leverkusen, Germany) was applied to the eyes and blood glucose concentration was measured from a micro-puncture of a peripheral vein (Contour XT, Bayer Vital, Leverkusen, Germany), followed by insertion of a 26G tail vein catheter into one of the lateral tail veins. Anesthetized animals were then transferred to a dedicated animal bed with integrated warming (Minerve, Esternay, France), and respiratory rate was continuously monitored (BioVet, m2m Imaging, Cleveland, OH, USA) throughout the whole imaging procedure. Two mice were imaged simultaneously (sideby-side) in one PET scan acquisition. During the scans, the isoflurane level was individually adjusted (1.0-2.5 % in oxygen) to achieve a constant depth of anesthesia, keeping the respiration rate at around 60-80 breaths/min. Animals were injected with 0.1 mL [18F]FDG solution and a 60-minute dynamic PET scan was initialized. The number of animals/PET acquisition, mean body weight and injected [18F]FDG activity at each of the imaging time points are summarized in Table 1. Immediately after completion of the PET scan, a second blood sample for glucose measurement was taken from the lateral tail vein, and the animal beds were transferred to a small animal CT scanner (Inveon CT, Siemens Medical Solutions, Knoxville, TN, USA), where a fast low-dose CT scan was performed to provide anatomical data for subsequent image analysis.

Dynamic PET emission data from the 60-minute scans were sorted into 32 time frames, incrementally increasing in time length from 5 s to 10 min (5  $\times$  2, 4  $\times$  5, 3  $\times$  10, 8  $\times$  30, 5  $\times$  60, 4  $\times$  300 and 3  $\times$  600 s). All PET images were reconstructed using an ordered subset expectation maximum fast maximum a posteriori algorithm (OSEM3D/fastMAP) using 2 iterations OSEM in 16 subsets and 18 iterative MAP ( $\beta=0.01$ ), resulting in a final voxel size of  $0.78\times0.78\times0.80$  mm $^3$ . The standard data correction protocol (normalization, attenuation, scatter, and decay correction) was applied to the PET data. Attenuation data was acquired from 10-minute external rotating Co-57 point source transmission scans. The PET units were converted into units of radioactivity by applying a

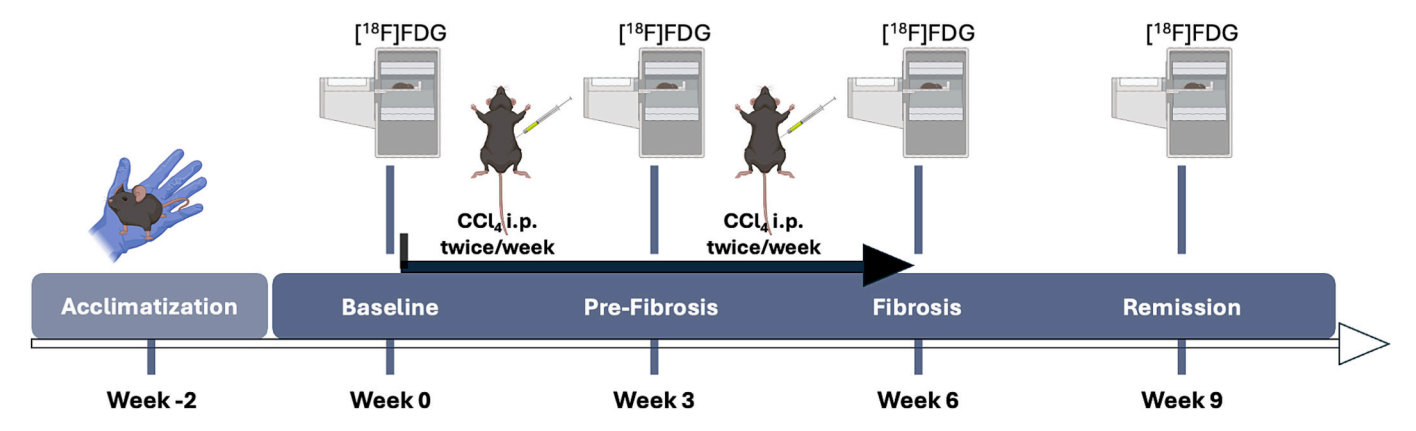


Fig. 1. Timeline of experiments. In male C57BL/6N mice (n = 7-10) dynamic, whole-body PET scans were acquired for 60 min after intravenous injection of [ $^{18}$ F] FDG at baseline, and subsequently in three-week intervals (pre-fibrosis, fibrosis, remission stages). Between the PET scans at baseline, pre-fibrosis and fibrosis stages, carbon tetrachloride (CCl<sub>4</sub>) was repeatedly administered intraperitoneally (i.p.) twice weekly. CCl<sub>4</sub> treatment was discontinued after the scans at fibrosis stage and remission PET scans were performed three weeks later at the end of the study.

**Table 1**Overview of animal numbers, body weight, and injected activity during the time course of the PET study.

Imaging time point	Number of PET acquisition	Body weight	Injected [ <sup>18</sup> F]FDG activity	Number of animals included in data analysis	
	n =	[g]	[MBq]	SUV / SUV <sub>gluc</sub>	PK- Modeling
				$\mathbf{n} =$	n =
Baseline	10	$23.4 \pm 0.5$	$12.4\pm0.8$	10	8ª
Pre- Fibrosis	10	$24.1\pm0.8$	$12.3\pm1.1$	10	8 <sup>a</sup>
Fibrosis	9	$24.7\pm1.1$	$11.7\pm1.0$	9	8 <sup>a</sup>
Remission	7	$27.5\pm1.4$	$11.7\pm0.7$	7	7

<sup>&</sup>lt;sup>a</sup> Remaining scans because obtained blood curve was not suitable for Patlak/ 2-tissue compartment modeling.

calibration factor, which was derived from measuring a cylindrical phantom with known [<sup>18</sup>F]FDG activity concentrations.

#### 2.3. Image analysis

Image analysis was performed by an experienced experimenter who was aware of the experimental study phase at time of [18F]FDG-PET. Brain uptake was assessed at 40-60 min post [18F]FDG-administration in various semi-quantitative parameters such as percent injected dose per cubic centimeter (%ID/cc), mean SUV and SUVgluc. Those values were subsequently compared with MRGlu, which represents the final phosphorylated and therefore intracellularly trapped amount of [<sup>18</sup>F] FDG. MR<sub>Glu</sub> was derived by Patlak or 2-tissue compartment modeling analysis of the dynamic (0-60 min) PET data. Image data were analyzed using PMOD 4.3 software (Pmod Technologies, Faellanden, Switzerland). The resulting PET images were co-registered to the respective CT images and the CT was then fused to a T2 MRI template [23]. Both transformation matrices were further combined to co-register the PET image to the MRI template and a mouse brain volume of interest (VOI) template [23] was applied on the dynamic images to derive timeactivity curves (TACs) from 0 to 60 min. Mean uptake at 40-60 min (last two PET frames) post-injection in whole brain and brain regions normalized to the injected dose of each VOI was calculated to yield data in the form of %ID/cc. Liver uptake was assessed on the co-registered whole-body PET/CT images by placing a  $4 \times 4 \times 4$  mm<sup>3</sup> box-shaped VOI in the liver region located on the opposite side to the stomach. SUVs were calculated using the following equation:

$$SUV = \frac{C_{PET}(T)}{A/W} \tag{1}$$

where  $C_{PET}(T)$  is the mean [ $^{18}$ F]FDG activity concentration in the respective time frame on the dynamic PET image, A is the total injected [ $^{18}$ F]FDG activity in MBq and W is the body weight of the respective animal in gram. SUV<sub>gluc</sub> were calculated as:

$$SUV_{gluc} = SUV \times C_{gluc} / 100 \tag{2}$$

where SUV is the standardized uptake value of the region of interest and  $C_{gluc}$  is the averaged blood glucose concentration in units of mg/dL (1 mmol/L  $\triangleq$  18.0182 mg/dL) measured before [ $^{18}$ F]FDG administration and at the end of the PET scan [13]. As established before, the vena cava was used as an image-derived input function (IDIF) for kinetic modeling by placement of a 2  $\times$  2  $\times$  4 mm VOI in the inferior vena cava superior to the renal branches [24]. For regional brain analysis, the vena cava TACs and TACs derived from selected brain regional VOIs were loaded together into the Pmod pkin tool and fitted to the Patlak model [12]. The glucose net influx rate ( $k_i$ ) was calculated from the slope of the Patlak plot. Subsequently,  $MR_{Glu}$  was calculated:

$$MR_{Glu} = k_i \times \frac{C_{gluc}}{IC} \tag{3}$$

where  $C_{gluc}$  is the averaged blood glucose concentration measured in blood and LC is the lumped constant (0.67) as estimated in mice [25]. Because glucose uptake in the brain tended to equilibrate at 2 min after administration and plateaued at frames after 20 min, only frames between 2 and 20 min were considered for the Patlak analysis [24,26]. For comparison, the standard two-tissue compartment model for [<sup>18</sup>F]FDG was also used and  $MR_{Glu}$  values were derived as follows:

$$MR_{Glu} = \frac{C_{gluc}}{LC} \times \frac{K_1 \times k_3}{k_2 + k_3} \tag{4}$$

where  $C_{gluc}$  is the averaged blood glucose concentration measured in blood, LC is the lumped constant (0.67) and  $K_1$ ,  $k_2$  and  $k_3$  were the fitted model parameters assuming a vascular blood fraction in the brain of 5 % and a slow rate of dephosphorylation ( $k_4 \cong 0$ ) [27].

The  $SUV_{gluc}$ —derived whole-brain maps were used for statistical parametric mapping (SPM) analysis using SPM 12 software (UCL, London, UK). Differences from baseline uptake were calculated by a two-tailed unpaired t-test with a significance level threshold of 0.05 (uncorrected for multiple comparisons) and a minimum cluster size of 50 voxels. After each comparison, the derived parametric t-maps were loaded into Pmod, and significantly changed voxels were located by co-

registration with the T2 MRI template [23]. The threshold of the t-maps was set according to the degrees of freedom of the respective comparisons.

#### 2.4. Statistical analysis

Statistical testing was performed using GraphPad Prism 10.2.3 software (GraphPad Software, La Jolla, CA, USA). Before statistical analysis, normal distribution of data was tested by Shapiro-Wilk test. Imaging parameters derived at baseline were considered as the reference values. Differences to baseline uptake were analyzed by ordinary one-way ANOVA followed by Dunnett's multiple comparisons test. Correlation analysis was performed using Pearson's correlation test. The level of statistical significance was set to p < 0.05. Data are presented as mean  $\pm$  standard deviation (SD) and individual data points.

#### 3. Results

## 3.1. CCl<sub>4</sub>-induced liver fibrosis differentially impacts brain and liver glucose metabolism

Of the eleven animals repeatedly imaged in random order in this study at baseline and pre-fibrosis, three animals were lost (due to weight-loss (humane end-point), a non-study-related injury, and an anesthesia incident). Five scans were excluded from the pharmacokinetic analyses as the blood input function could not be fitted properly (Table 1). Mean whole-brain TACs for the 60-minute scan in %ID/cc, SUV and blood-glucose corrected SUV $_{\rm gluc}$  from the investigated animals are presented in Fig. 2.

The blood glucose levels assessed during the time course of the study are depicted in Fig. 3. The averaged blood glucose concentration varied during the disease stages and were  $9.02\pm1.30$  mmol/L at baseline, dropped to  $5.82\pm1.59$  (p <0.0001) and  $5.81\pm1.47$  (p <0.0001) mmol/L at pre-fibrosis and fibrosis, respectively, and recovered in the remission stage to values comparable to baseline ( $9.83\pm1.03$  mmol/L; p =0.515; Fig. 3a). The blood glucose levels measured before [ $^{18}$ F]FDG administration followed a similar pattern with  $10.75\pm0.90$  mmol/L at baseline, followed by a decrease to  $7.27\pm1.60$  (p <0.0001),  $6.74\pm1.60$ 

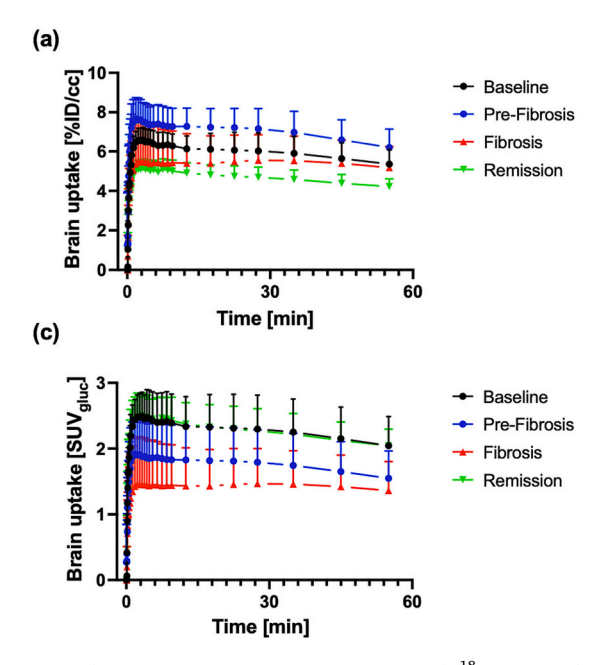
1.63~(p<0.0001) and an increase to  $10.20\pm1.14~mmol/L~(p=0.755)$  at pre-fibrosis, fibrosis and remission stage, respectively (Fig. 3b). Conversantly, at the end of the PET scan, blood glucose levels were generally lower and showed higher variability, with  $7.23\pm2.53~mmol/L$  at baseline and  $4.34\pm1.76~(p=0.011),\,5.28\pm1.89~(p=0.127)$  and  $9.43\pm2.09~mmol/L~(p=0.104)$  at pre-fibrosis, fibrosis and remission stage, respectively (Fig. 3c).

Mean TACs for the liver obtained from the 60 min [ $^{18}$ F]FDG PET scan at the investigated stages in units of SUV are shown in Fig. 4a. Uptake of [ $^{18}$ F]FDG at 40–60 min after administration increased from baseline (0.58  $\pm$  0.07 SUV) to pre-fibrosis (0.86  $\pm$  0.20 SUV; p = 0.0005) and fibrosis stage (0.82  $\pm$  0.19 SUV; p = 0.003; Fig. 4b). At remission, [ $^{18}$ F] FDG liver uptake was comparable to baseline again (0.61  $\pm$  0.04 SUV; p = 0.956). Masson's trichrome staining of liver tissue confirmed increase of collagen deposition, indicative of fibrotic tissue development during the different stages of the study (Fig. 4c).

Averaged, brain maps co-registered to the MRI brain atlas showing [18F]FDG uptake at 40-60 min, corrected for body weight and blood glucose levels (SUV<sub>gluc</sub>) in male C57BL6/N mice at baseline, pre-fibrosis, fibrosis and remission stages are shown in Fig. 5a. Here, a significant global decrease in  $SUV_{gluc}$ , indicative of a pronounced glucose hypometabolism, was observed during pre-fibrosis (1.60  $\pm$  0.43; p = 0.03) and fibrosis stages (1.39  $\pm$  0.46; p = 0.003) compared to baseline (2.1  $\pm$  0.46). At remission, SUV $_{gluc}$  values returned to baseline levels, suggesting reversible processes at this stage (2.09  $\pm$  0.26; p = 0.999; Fig. 5b). SPM analysis further revealed brain regions with a more pronounced decrease in SUV<sub>gluc</sub> compared to baseline, which included cortical and hippocampal regions at pre-fibrosis and, additionally, striatal, thalamic and cerebellar regions at the fibrosis stage (Fig. 5c). Accordingly, SUV<sub>gluc</sub> values in striatum, cortex, hippocampus, thalamus, amygdala and cerebellum acquired from atlas-based regional analysis showed a progressive decrease from pre-fibrosis to fibrosis stage, which was fully restored to baseline after remission (Fig. S1).

#### 3.2. $MR_{Glu}$ correlates with $SUV_{gluc}$ , but not with SUV

An IDIF derived from the inferior vena cava of each animal and the respective averaged blood glucose values, assessed before and at the end



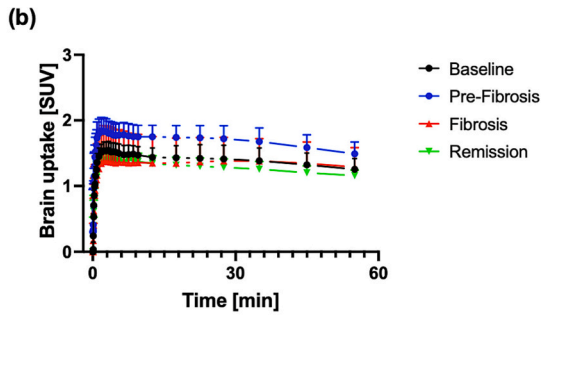


Fig. 2. Mean time-radioactivity concentration curves (TACs) of [ $^{18}$ F]FDG uptake in the whole-brain of male C57Bl6/N mice expressed as (a) percent injected dose per mL (%ID/cc), (b) body weight normalized standardized uptake value (SUV), and (c) the blood-glucose normalized standardized uptake value (SUV  $_{gluc}$ ). SUV and SUV  $_{gluc}$  data were derived from the %ID/cc data according to the formulas (1) and (2) as listed in the Material and Methods part. Data are shown as mean + SD (n = 7–10 animals per imaging time point).

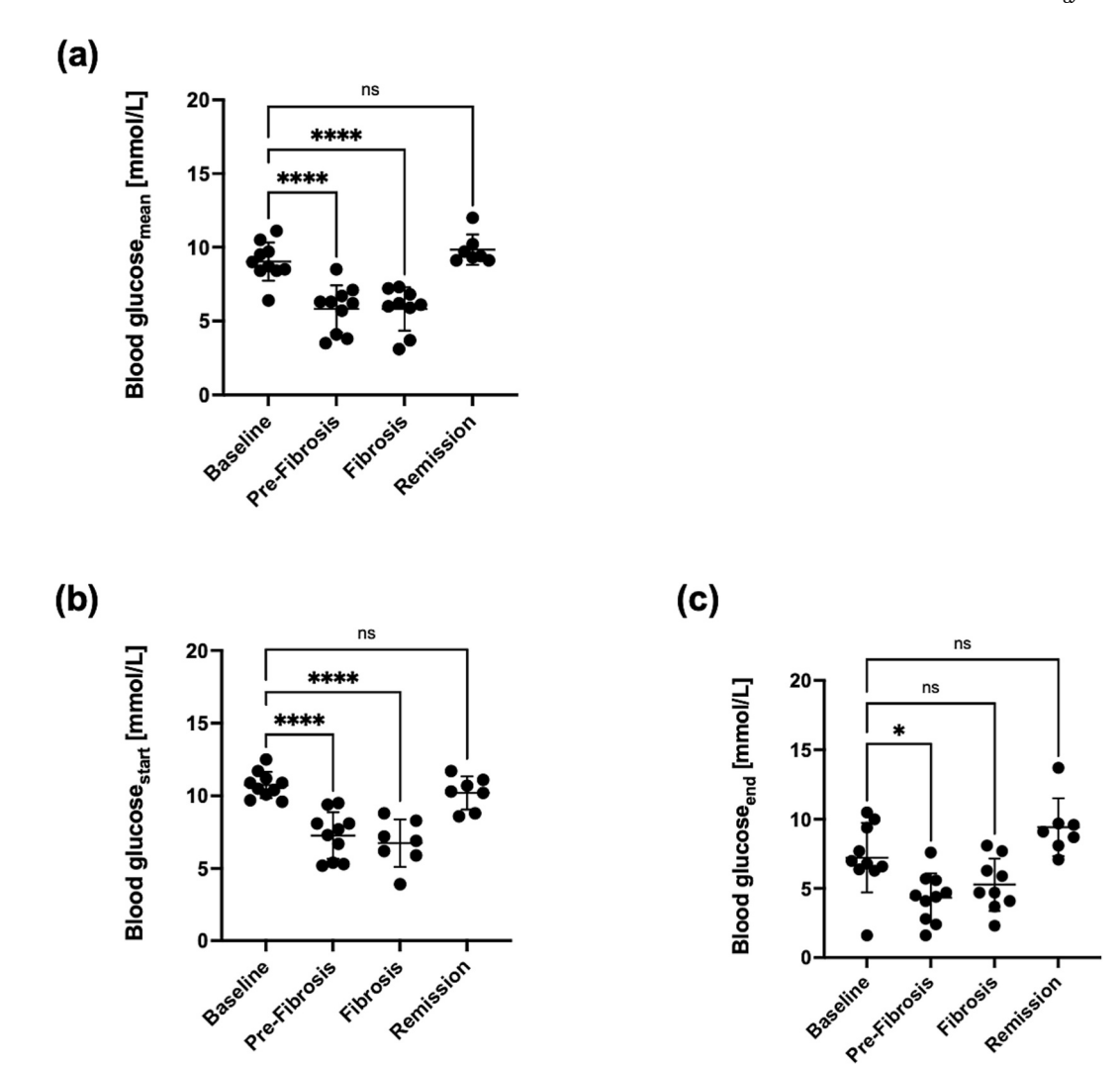


Fig. 3. Averaged blood glucose levels (a), calculated from the measurements before [ $^{18}$ F]FDG administration and at the end of the PET scan as well as blood glucose levels directly before start of the imaging procedure (b) and at the end of the 60-minute PET acquisition (c) in male C57BL/6N mice (n = 7–10). Data are expressed as mean  $\pm$  SD. Statistical differences were assessed by one-way ANOVA followed by Dunnett's multiple comparison test. \*p < 0.05, \*\*p < 0.01, \*\*\*p < 0.001, \*\*\*\*p < 0.0001.

of [18F]FDG PET, were used to calculate MR<sub>Glu</sub> using both, the Patlak and the 2-tissue compartment model for [18F]FDG. Expectedly, comparing MR<sub>Glu</sub> values derived from Patlak analysis to values derived from the 2-tissue compartment model for FDG resulted in a very strong correlation ( $R^2 = 0.98$ ; p < 0.0001), as assessed by Pearson correlation test (Fig. S2). Compared to baseline, Patlak-derived MR $_{Glu}$  (27.27  $\pm$ 7.63 µmol/min/100 g) values decreased significantly at pre-fibrosis (16.09  $\pm$  6.81 µmol/min/100 g; p = 0.008) and fibrosis (16.41  $\pm$  $3.31 \ \mu mol/min/100 \ g; \ p = 0.010)$  and returned to the initial values at the remission stage (32.56  $\pm$  8.50  $\mu$ mol/min/100 g; p = 0.323; Fig. 6a). The 2-tissue compartment model for [18F]FDG yielded comparable  $MR_{Glu}$  values with 28.19  $\pm$  8.92  $\mu mol/min/100$  g at baseline, and a significant decrease at pre-fibrosis (16.09  $\pm$  7.05  $\mu$ mol/min/100 g; p = 0.009) and fibrosis stages (16.32  $\pm$  3.30  $\mu mol/min/100$  g; p = 0.010) followed by a return to the initial values at remission (32.04  $\pm$  9.28  $\mu mol/min/100$  g; p = 0.634; Fig. 6b). The calculated MR<sub>Glu</sub> showed a positive correlation to the surrogate parameter SUV<sub>gluc</sub>, irrespective if derived from Patlak analysis ( $R^2 = 0.46$ ; p < 0.001; Fig. 6d) or from the 2-tissue compartment model for  $[^{18}F]FDG$  ( $R^2 = 0.47$ ; p < 0.001; Fig. 6e). In contrast, brain uptake of [18F]FDG expressed as SUV only  $(1.29 \pm 0.17 \text{ at baseline vs. } 1.53 \pm 0.19 \text{ at pre-fibrosis; } p = 0.031; 1.32$  $\pm$  0.31 and 1.18  $\pm$  0.09 SUV at fibrosis and remission, respectively; Fig. 6c) did not correlate with the SUV<sub>gluc</sub> values ( $R^2 = 0.004$ ; p = 0.28;

Fig. 6f). This absence of correlation was independent from the time point of blood glucose sampling and did not change when  $C_{gluc}$  was not averaged as indicated in eq. (2) but taken from the first blood glucose measurement to calculate  $SUV_{gluc}(SUV_{gluc}Start)$  or at the end of the PET scan  $(SUV_{gluc}End; Fig. S3a,b)$ .

Furthermore, whole-brain SUV values did not correlate to  $MR_{Glu}$  or net influx rate  $(k_i)$  values, irrespective if the Patlak model  $(R^2=0.07; p=0.20 \text{ for } MR_{Glu}; R^2 < 0.001; p=0.99 \text{ for } k_i)$  or the 2-tissue compartment model for  $[^{18}F]FDG$   $(R^2=0.04; p=0.35 \text{ for } MR_{Glu}; R^2 < 0.001; p=0.97 \text{ for } k_i)$  were used (Fig. S4a-e). Further pharmacokinetic model parameters, such as the net influx rate  $(k_i)$  of  $[^{18}F]FDG$  did not show any significant changes from baseline at all assessed time points, irrespective if derived from Patlak analysis (Fig. S5a) or the 2-tissue compartment model (Fig. S5b). Similarly, the first-order rate constant depicting capillary transport of  $[^{18}F]FDG$  into the brain parenchyma  $(K_I)$  as well the rate constants  $k_2$  and  $k_3$  in the 2-tissue compartment model did not change at the investigated imaging time points (Table 2; Fig. S5c). Consequently, neither  $k_i$  nor  $K_I$  correlated with the SUV<sub>gluc</sub> values derived in this study (Fig. S5d-f).

#### 4. Discussion

The first aim of this study was to identify, to our knowledge for the

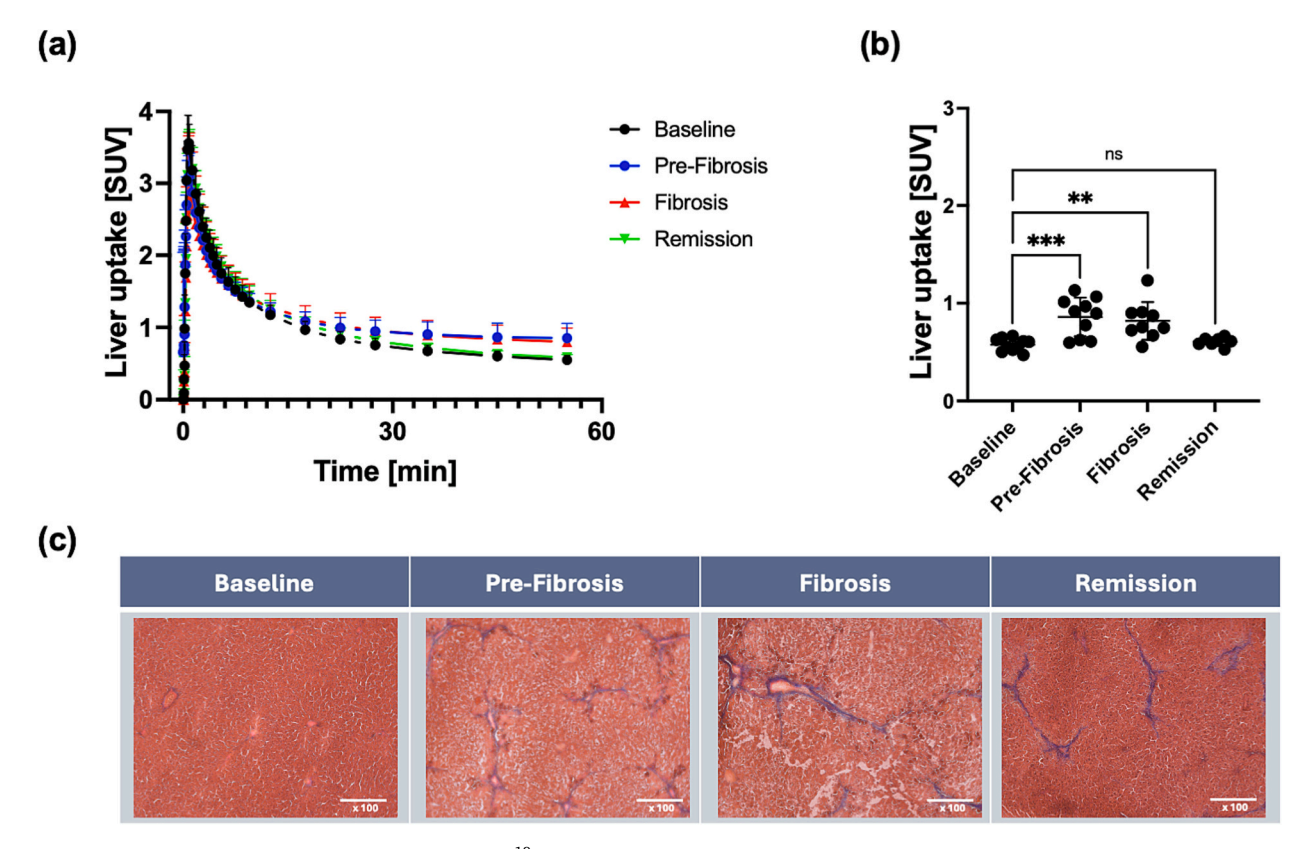


Fig. 4. Mean time-radioactivity concentration curves (TACs) of  $[^{18}F]$ FDG uptake in the liver (a) during the 60-minute PET scan in male C57Bl6/N mice expressed in units of SUV. Panel (b) shows corresponding quantification for the 40–60 min interval after i.v. administration of  $[^{18}F]$ FDG. Masson's trichrome staining of liver tissue at x100 magnification (c) showing increased collagen deposition (blue color), indicative of fibrotic tissue development across the different stages of the study. Data are shown as mean + SD (n = 7–10 animals per imaging time point). Statistical differences were assessed by one-way ANOVA followed by Dunnett's multiple comparison test.  $^*p < 0.05$ ,  $^*p < 0.01$ ,  $^{***}p < 0.001$ ,  $^{***}p < 0.001$ ,  $^{***}p < 0.0001$ . (For interpretation of the references to color in this figure legend, the reader is referred to the web version of this article.)

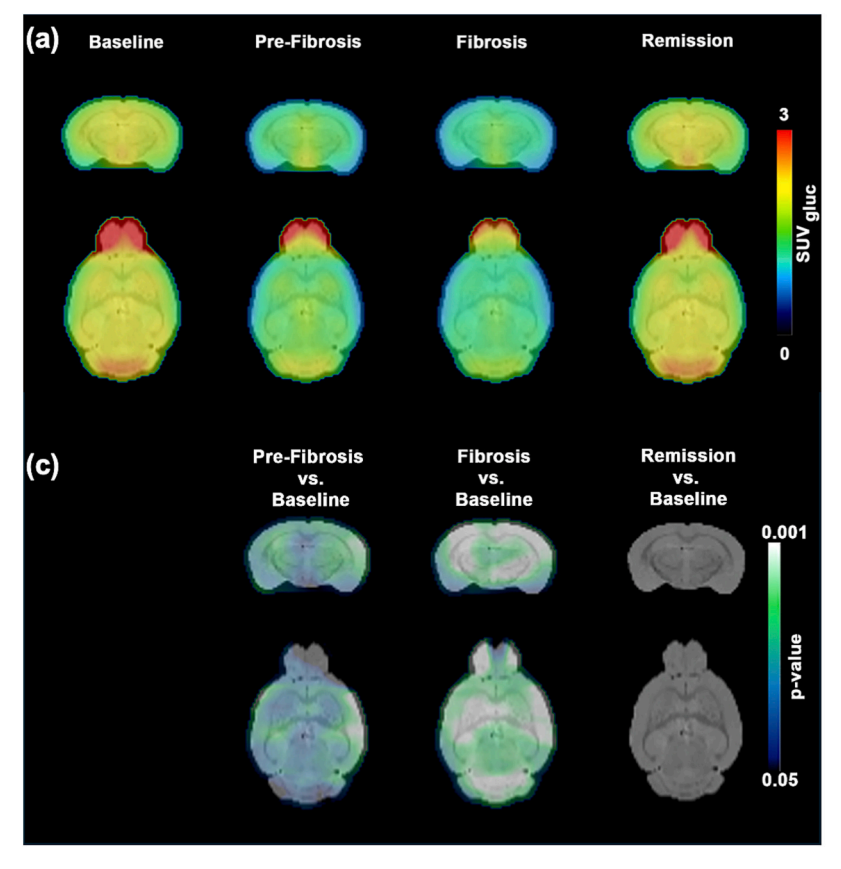
first time, cerebral glucometabolic changes during liver fibrosis progression in a well-established mouse model of CCL<sub>d</sub>-induced liver fibrosis, using [18F]FDG PET imaging. The second aim was to validate  $SUV_{gluc}$  as a surrogate parameter for cerebral glucose metabolism (see below), which would be advantageous as SUVgluc does not require dynamic PET scans or a blood input curve, unlike the gold standard  $MR_{Gh}$ . Originally, the study was designed to investigate pathological changes in the liver in mice following exposure to a toxic challenge using various radiotracers, including [18F]FDG [19]. Given that the PET scanner's field of view was sufficiently wide to capture almost the entire mouse body, we expanded our analysis to include the brain. Our interest focused on assessing potential alterations in cerebral glucose metabolism across different stages of CCl4-induced liver fibrosis. To this end, we retrospectively analyzed dynamic [18F]FDG PET images and compared several quantitative parameters of [18F]FDG and glucose turnover. Our data reveal signs of impaired liver-brain metabolic coupling in terms of a pronounced glucose hypometabolism affecting the entire brain during the progression of liver fibrosis. This decline in brain glucose consumption was reversible, with glucose uptake returning to baseline levels within three weeks following the cessation of CCl<sub>4</sub> treatment. Cerebral glucohypometabolism assessed by [18F]FDG PET is one of the early diagnostic markers for mild cognitive impairment and conversion to Alzheimer's disease in human patients [28–30]. Recently, an association between liver fibrosis and worse performance in cognitive tests was reported in humans [31], and further, the severity of liver fibrosis may serve as a risk factor for dementia [32]. While changes in brain glucometabolism, to our knowledge, remain to be investigated in patients with liver fibrosis, the glucohypometabolism found here could indicate a possible connection between the disease and cognitive

impairment. Preclinical studies that examine the potential interaction between liver fibrosis and cognitive function in parallel to glucose metabolism would therefore certainly be of clinical interest and relevance.

Apart from its fibrotic effects in the liver, CCl<sub>4</sub> can exert toxic effects on various tissues, including the brain, as a consequence of free radical formation and oxidative stress [33]. It therefore needs to be considered that CCl<sub>4</sub> treatment per se might have impacted cerebral glucometabolism in consequence of cellular damage in the present study. As no histological examination was undertaken, we cannot exclude that, e.g. inflammatory reactions of the brain in terms of glial activation were present in the mice as a consequence of CCl<sub>4</sub> exposure. However, if this was the case, one would expect an increase in glucose metabolism rather than the observed decrease. Literature regarding intraperitoneal administration of CCl<sub>4</sub> being harmful to the brain is lacking. It has been shown, that chronic inhalation exposure (400 ppm, 8 h/day, 5d/week for >10 months) did not induce changes in activity, alertness, or appetite in rats [34] whereas shorter and lower-dose exposure (180 ppm, 15 in/d, 2d/week for 8 weeks) resulted in liver fibrosis [35]. Further, oral administration of up to 1.6 g/kg/week, a similar dose compared to the mouse data presented here, for 10 weeks induced diffuse liver cirrhosis and increased serotonin levels in the rat brain, but these were not associated with abnormal behavior in the open field test [36]. Therefore, direct neurotoxic effects of CCl4 treatment are unlikely the cause of our observed findings.

To quantify glucose utilization in the brain, we employed  $SUV_{gluc}$  and validated its correlation with  $MR_{Glub}$  as determined through multiple kinetic modeling approaches. Kinetic modeling with an input function represents the gold standard for converting [ $^{18}$ F]FDG uptake values

(b)



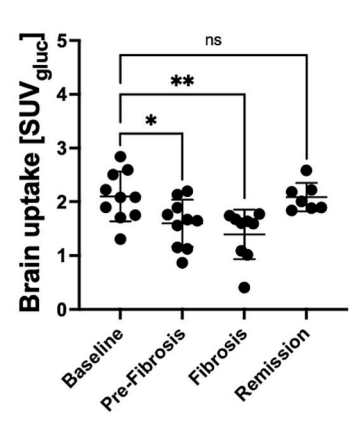
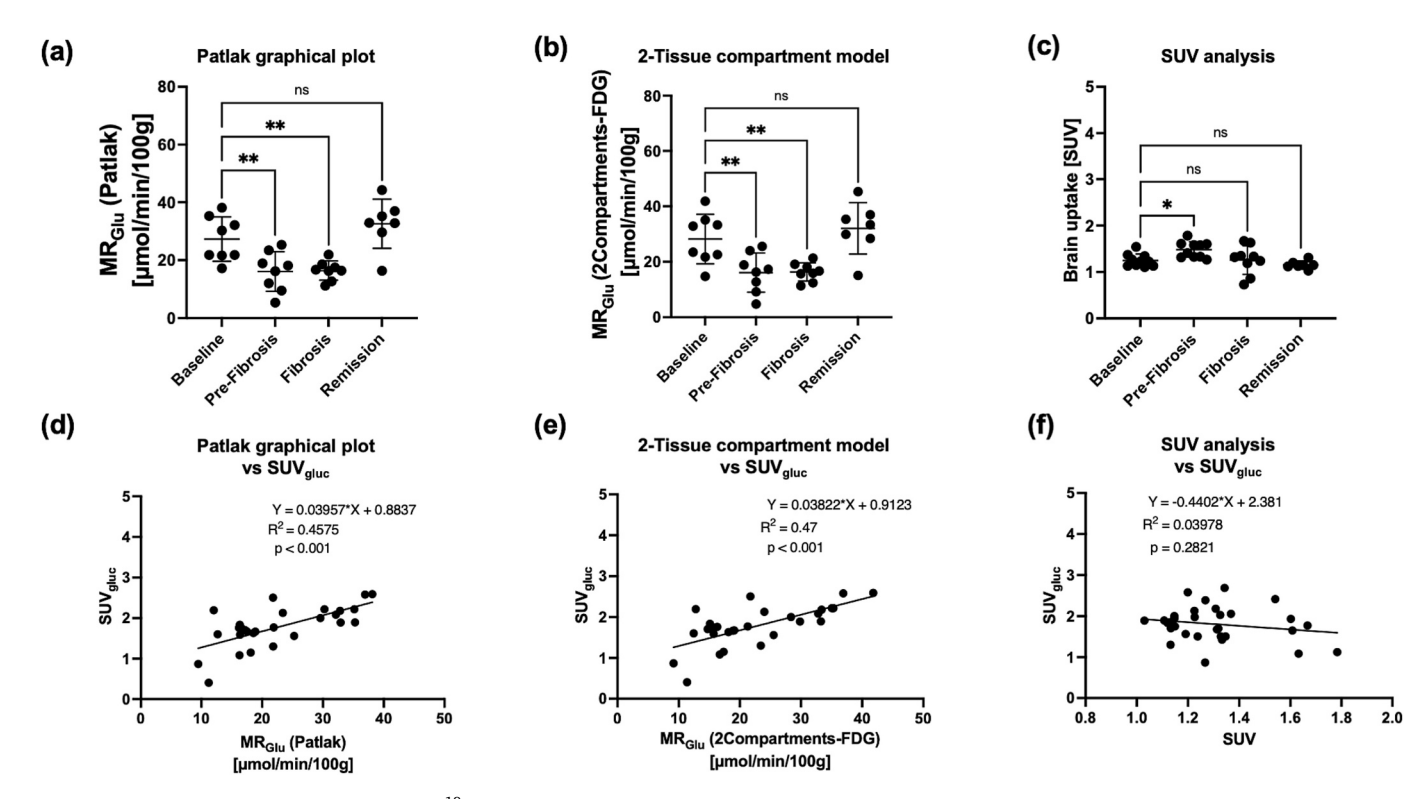


Fig. 5. (a) Averaged coronal ( $\sim$ 2.2 mm caudal to bregma) and horizontal ( $\sim$ 5.0 mm ventral to bregma) blood-glucose normalized standardized uptake value ( $SUV_{gluc}$ ) brain maps of [ $^{18}$ F]FDG and (b) respective quantification at 40–60 min after i.v. administration in male C57BL/6N mice (n = 7–10 subjects per imaging time point) at baseline, pre-fibrosis, fibrosis, and remission. In (c) coronal and horizontal statistical parametric mapping (SPM) t-maps resulting from voxel-wise comparison of baseline condition with uptake at pre-fibrosis, fibrosis and remission stages are shown. Only clusters with significantly different voxels from baseline are shown (Student's t-test, p < 0.05, minimum cluster size 50 voxels). The scale bar represents significantly decreased p-values for each voxel compared to baseline. Data are expressed as mean  $\pm$  SD. Statistical differences were assessed by one-way ANOVA followed by Dunnett's multiple comparison test. \*p < 0.05, \*\*p < 0.01, \*\*\*\*p < 0.001.

from PET scans into  $MR_{Glu}$ . However, in mouse studies, obtaining the input function is technically challenging due to the limited blood volume available. While catheterization of the femoral or jugular artery is feasible in non-recovery studies, such invasive procedures are unsuitable for longitudinal or interventional imaging setups as they preclude repeated scanning of the same animal. To overcome the technical challenges associated with invasive surgeries, IDIF methods have been developed [24,25,37]. These methods demonstrate excellent robustness for Patlak and two-compartment modeling approaches. However, generating an IDIF requires additional image analysis and is restricted to dynamic PET acquisitions, both of which limit overall imaging throughput. To address these limitations, we utilized brain SUV<sub>gluc</sub> in non-fasted mice as the primary outcome measure in this study. Originally introduced for the investigation of CNS lesions, SUVgluc offers significant advantages: it circumvents the need for complex kinetic modeling, eliminates the requirement for an IDIF, and can be calculated from static PET acquisitions [13]. Still, to convert SUV into SUV<sub>gluc</sub>, accurate data on blood glucose levels are required. We deliberately omitted fasting periods before the [18F]FDG PET scans, as prolonged fasting imposes a higher severity burden, particularly in diseased mice, presents significant organizational challenges for most imaging laboratories, and is technically difficult to standardize. Instead, blood glucose concentrations were measured in isoflurane-anesthetized mice immediately before [18F]FDG administration and again after the PET scan at standardized intervals using the same type of glucometer. A recent study confirmed an excellent agreement of the employed glucometers with blood glucose measurements from a certified lab [38]. The two measurements were averaged to approximate the blood glucose concentration during the entire imaging procedure. We favor averaging two blood glucose measurements over one because this approach alleviates the influence of prolonged isoflurane anesthesia on blood glucose levels (Fig. 3). To validate the suitability of brain  $SUV_{gluc}$  for static imaging, we used only the last two time frames of the dynamic PET data for the conversion. These time frames corresponded to the interval between 40 and 60 min post-[ $^{18}$ F]FDG administration, which aligns with the time-frame typically used in static [ $^{18}$ F]FDG PET scans [ $^{39}$ ], due to a relatively stable [ $^{18}$ F]FDG signal in this interval.

Following our methodology, we observed significant correlations between the individual whole-brain  $SUV_{gluc}$  and  $MR_{Glu}$  values in the investigated mice, regardless of whether  $MR_{Glu}$  was derived using Patlak analysis or 2-compartment kinetic modeling. Notably,  $MR_{Glu}$  values obtained via Patlak analysis exhibited a strong correlation with those derived from the 2-compartment model, despite the Patlak method considering only the 2 to 20-minute time interval post-[ $^{18}$ F]FDG injection. This might be different in situations where the rate constant  $k_3$  is affected, which was not the case in our study (Table 2). These findings suggest that if  $k_3$  is unaltered, Patlak analysis can be favored for quantifying cerebral glucose consumption due to its methodological simplicity and the possibility of utilizing a shorter PET acquisition protocol. Of note, neither the net influx rate  $k_i$  nor the influx rate constant  $K_1$ , showed any correlation to the derived SUV $_{gluc}$  values in our study.

Conflicting reports exist regarding the correlation between  $SUV_{gluc}$  and  $MR_{Glu}$ , with some studies demonstrating a correlation [40,41] while



**Fig. 6.** Kinetic analysis of whole-brain dynamic [ $^{18}$ F]FDG PET data and correlation to blood-glucose corrected standardized uptake value ( $SUV_{gluc}$ ). Metabolic rate of glucose ( $MR_{Glu}$ ) calculated by ( $\mathbf{a}$ ,  $\mathbf{d}$ ) Patlak graphical plot analysis and ( $\mathbf{b}$ ,  $\mathbf{e}$ ) 2-tissue compartment model for [ $^{18}$ F]FDG, as well as whole-brain uptake, expressed as standardized uptake values (SUV) and correlation analysis ( $\mathbf{c}$ ,  $\mathbf{f}$ ) at 40–60 min after i.v. administration in male C57BL/6N mice (n=7-10 subjects per imaging time point) at baseline, pre-fibrosis, fibrosis, and remission stages. Data are expressed as mean  $\pm$  SD. Statistical differences were assessed by one-way ANOVA followed by Dunnett's multiple comparison test. \*p < 0.05, \*\*p < 0.01, \*\*\*p < 0.001, \*\*\*\*p < 0.0001. R<sup>2</sup> and p values were calculated by Pearson correlation test.

**Table 2** Calculated mean  $K_1$ ,  $k_2$  and  $k_3$  rate constants, derived from the 2-tissue compartment model for [<sup>18</sup>F]FDG during the time course of the PET study.

Imaging time point	<u>K<sub>1</sub></u>	<u>k<sub>2</sub></u>	<u>k</u> <sub>3</sub>
	[ml/cc/min]	[1/min]	[1/min]
Baseline Pre-Fibrosis Fibrosis Remission	$\begin{aligned} 1.03 &\pm 0.24 \\ 1.12 &\pm 0.28 \\ 0.94 &\pm 0.29 \\ 0.93 &\pm 0.22 \end{aligned}$	$\begin{array}{c} 0.78 \pm 0.17 \\ 0.72 \pm 0.17 \\ 0.62 \pm 0.19 \\ 0.78 \pm 0.25 \end{array}$	$\begin{array}{c} 0.019 \pm 0.011 \\ 0.017 \pm 0.012 \\ 0.014 \pm 0.002 \\ 0.020 \pm 0.009 \end{array}$

Data are expressed as mean  $\pm$  SD.

others do not [42,43]. It is important to acknowledge that factors such as animal mobility during awake uptake or feeding conditions may introduce variability into [ $^{18}\mathrm{F}]\mathrm{FDG}$  uptake. Discrepancies between studies may reflect the sensitivity of  $SUV_{gluc}$  calculations to specific study setups, emphasizing the critical role of standardized imaging protocols within individual imaging institutions. As such, a universal conclusion on the favorability of one quantification method over another cannot be made and requires validation through correlation studies tailored to each imaging institution's capabilities. In our study, [ $^{18}\mathrm{F}]\mathrm{FDG}$  uptake took place under controlled conditions, specifically under continuous breathing-rate adjusted isoflurane anesthesia. SUV and subsequent  $SUV_{gluc}$  values were derived from data obtained through dynamic PET acquisition.

A factor to consider when utilizing *SUV* values is the body weight, as individual body weight is used to convert PET data into *SUV* units. Although no untreated control group was part of the present study, the body weight development of the mice (Table 1) corresponded to the respective data of male C57BL/6N mice from the breeder (www.criver.com), suggesting it remained largely unaffected by fibrosis

development. Further, the relative variability in body weight between imaging time points was minimal (ranging from 2 % to 5 %), and the overall increase in body weight from baseline to remission was 18.4  $\pm$  3.9 % (Table 1).

Conversely, our data highlight the unsuitability of the SUV as a standalone quantitative parameter for assessing cerebral glucose consumption in non-fasted mice. SUV showed no correlation with  $SUV_{gluc}$ , regardless of whether the blood glucose concentration used for the SUV-to- $SUV_{gluc}$  conversion was taken at the start, the end, or averaged from both measurements. More critically, SUV did not correlate with any modeling parameters, including  $MR_{Glu}$ , the net influx rate  $(k_1)$  or the influx rate constant  $(K_1)$ , irrespective of the pharmacokinetic model applied. These findings emphasize that, in a preclinical setting, conclusions regarding cerebral glucose metabolism should not be based solely on  $[^{18}F]FDG$  SUV (or % ID per cc tissue) values.

#### 5. Conclusions

In conclusion, our data reveal a significant decline in brain glucose metabolism during the progression of liver fibrosis. Notably, this hypometabolism was reversible, with glucose uptake returning to baseline within three weeks after discontinuing CCl<sub>4</sub> treatment. The observed reduction in brain metabolism may align with the reported association between liver fibrosis and impaired cognitive performance in human patients. Moreover, our study demonstrated strong correlations between individual whole-brain  $SUV_{gluc}$  and  $MR_{Glu}$  values in the investigated mice, regardless of whether  $MR_{Glu}$  was derived using Patlak analysis or 2-compartment kinetic modeling. This finding further supports the use of  $SUV_{gluc}$  as surrogate parameter for brain glucose metabolism in mice which is generally easier to obtain and does not require dynamic PET imaging and subsequent pharmacokinetic modeling. Of relevance, our findings also emphasize the limitations of the SUV as a

standalone quantitative measure for assessing cerebral glucose metabolism in non-fasted mice.

#### CRediT authorship contribution statement

Thomas Wanek: Writing – original draft, Visualization, Methodology, Investigation, Funding acquisition, Formal analysis, Data curation, Conceptualization. Mari Teuter: Writing – review & editing, Methodology, Investigation, Formal analysis. Asha Balakrishnan: Writing – review & editing, Supervision, Resources, Investigation. Tobias L. Ross: Writing – review & editing, Resources, Investigation. Frank M. Bengel: Writing – review & editing, Resources. Michael Ott: Writing – review & editing, Supervision, Resources. Marion Bankstahl: Writing – review & editing, Supervision, Project administration, Methodology, Investigation. Jens P. Bankstahl: Writing – original draft, Supervision, Project administration, Methodology, Investigation, Conceptualization.

#### Declaration of competing interest

The authors declare that they have no known competing financial interests or personal relationships that could have appeared to influence the work reported in this paper.

#### Acknowledgments

This work was supported by the COST action "Correlated Multimodal Imaging in Life Sciences" (COMULIS) via a Short- Term Scientific Mission (STSM) grant awarded to Thomas Wanek (E-COST-GRANT-CA17121-9d2090ba) and a Vienna School of Radiology (VISOR) mobility grant awarded to Thomas Wanek. The authors further thank A. Sander, P. Felsch and D. Ahrens for their skillful assistance. Some image content of this publication was created with BioRender.com.

#### References

- Matsubara Y, Kiyohara H, Teratani T, Mikami Y, Kanai T. Organ and brain crosstalk: the liver-brain axis in gastrointestinal, liver, and pancreatic diseases. Neuropharmacology 2022;205:108915.
- [2] Ribeiro IMR, Antunes VR. The role of insulin at brain-liver axis in the control of glucose production. Am J Physiol Gastrointest Liver Physiol 2018;315:G538–43.
- [3] Zolin A, Zhang C, Ooi H, Sarva H, Kamel H, Parikh NS. Association of liver fibrosis with cognitive decline in Parkinson's disease. J Clin Neurosci 2024;119:10–6.
- [4] Jiang R, Wu J, Rosenblatt M, Dai W, Rodriguez RX, Sui J, et al. Elevated C-reactive protein mediates the liver-brain axis: a preliminary study. EBioMedicine 2023;93: 104679
- [5] Bataller R, Brenner DA. Liver fibrosis. J Clin Invest 2005;115:209-18.
- [6] Parikh NS, Kumar S, Rosenblatt R, Zhao C, Cohen DE, Iadecola C, et al. Association between liver fibrosis and cognition in a nationally representative sample of older adults. Eur J Neurol 2020;27:1895–903.
- [7] Phelps ME. PET: a biological imaging technique. Neurochem Res 1991;16:929–40.
- [8] Mosconi L. Brain glucose metabolism in the early and specific diagnosis of Alzheimer's disease. FDG-PET studies in MCI and AD. Eur J Nucl Med Mol Imaging 2005;32:486–510.
- [9] Basset-Sagarminaga J, van de Weijer T, Iozzo P, Schrauwen P, Schrauwen-Hinderling V. Advances and challenges in measuring hepatic glucose uptake with FDG PET: implications for diabetes research. Diabetologia 2024;67:407–19.
- [10] Zhang W, Ning N, Li X, Li M, Duan X, Guo Y, et al. Impaired brain glucose metabolism in cirrhosis without overt hepatic encephalopathy: a retrospective 18F-FDG PET/CT study. Neuroreport 2019;30:776–82.
- [11] Phelps ME, Huang SC, Hoffman EJ, Selin C, Sokoloff L, Kuhl DE. Tomographic measurement of local cerebral glucose metabolic rate in humans with (F-18)2fluoro-2-deoxy-D-glucose: validation of method. Ann Neurol 1979;6:371–88.
- [12] Patlak CS, Blasberg RG, Fenstermacher JD. Graphical evaluation of blood-to-brain transfer constants from multiple-time uptake data. J Cereb Blood Flow Metab
- [13] Nozawa A, Rivandi AH, Kesari S, Hoh CK. Glucose corrected standardized uptake value (SUVgluc) in the evaluation of brain lesions with 18F-FDG PET. Eur J Nucl Med Mol Imaging 2013;40:997–1004.
- [14] Lee SM, Kim TS, Lee JW, Kim SK, Park SJ, Han SS. Improved prognostic value of standardized uptake value corrected for blood glucose level in pancreatic cancer using F-18 FDG PET. Clin Nucl Med 2011;36:331–6.
- [15] Jahromi AH, Moradi F, Hoh CK. Glucose-corrected standardized uptake value (SUV (gluc)) is the most accurate SUV parameter for evaluation of pulmonary nodules. Am J Nucl Med Mol Imaging 2019;9:243–7.

- [16] Deleye S, Verhaeghe J, Wyffels L, Dedeurwaerdere S, Stroobants S, Staelens S. Towards a reproducible protocol for repetitive and semi-quantitative rat brain imaging with (18)F-FDG: exemplified in a memantine pharmacological challenge. Neuroimage 2014;96:276–87.
- [17] Herfert K, Mannheim JG, Kuebler L, Marciano S, Amend M, Parl C, et al. Quantitative rodent brain receptor imaging. Mol Imaging Biol 2020;22:223–44.
- [18] Matthews PM, Coatney R, Alsaid H, Jucker B, Ashworth S, Parker C, et al. Technologies: preclinical imaging for drug development. Drug Discov Today Technol 2013;10:e343–50.
- [19] Teuter M, Balakrishnan A, Al-Bazaz S, Willmann M, Ott M, Bengel FM, et al. Serial multi-tracer PET/CT for characterization of CCl4-induced liver fibrosis in mice. J Nucl Med 2023;64. P1139-P.
- [20] Percie du Sert N, Hurst V, Ahluwalia A, Alam S, Avey MT, Baker M, et al. The ARRIVE guidelines 2.0: updated guidelines for reporting animal research. PLoS Biol 2020:18:e3000410.
- [21] Yang T, Poenisch M, Khanal R, Hu Q, Dai Z, Li R, et al. Therapeutic HNF4A mRNA attenuates liver fibrosis in a preclinical model. J Hepatol 2021;75:1420–33.
- [22] Scholten D, Trebicka J, Liedtke C, Weiskirchen R. The carbon tetrachloride model in mice. Lab Anim 2015;49:4–11.
- [23] Mirrione MM, Schiffer WK, Fowler JS, Alexoff DL, Dewey SL, Tsirka SE. A novel approach for imaging brain-behavior relationships in mice reveals unexpected metabolic patterns during seizures in the absence of tissue plasminogen activator. Neuroimage 2007;38:34–42.
- [24] Bascunana P, Thackeray JT, Bankstahl M, Bengel FM, Bankstahl JP. Anesthesia and preconditioning induced changes in mouse brain [(18)F] FDG uptake and kinetics. Mol Imaging Biol 2019;21:1089–96.
- [25] Yu AS, Lin HD, Huang SC, Phelps ME, Wu HM. Quantification of cerebral glucose metabolic rate in mice using 18F-FDG and small-animal PET. J Nucl Med 2009;50: 966-73
- [26] Wirth A, Wolf B, Huang CK, Glage S, Hofer SJ, Bankstahl M, et al. Novel aspects of age-protection by spermidine supplementation are associated with preserved telomere length. Geroscience 2021;43:673–90.
- [27] Reivich M, Kuhl D, Wolf A, Greenberg J, Phelps M, Ido T, et al. The [18F] fluorodeoxyglucose method for the measurement of local cerebral glucose utilization in man. Circ Res 1979;44:127–37.
- [28] Liu F, Shi Y, Wu Q, Chen H, Wang Y, Cai L, et al. The value of FDG combined with PiB PET in the diagnosis of patients with cognitive impairment in a memory clinic. CNS Neurosci Ther 2024;30:e14418.
- [29] Zhu L, Zhao W, Chen J, Li G, Qu J. Systematic review and meta-analysis of diagnostic test accuracy (DTA) studies: the role of cerebral perfusion imaging in prognosis evaluation of mild cognitive impairment. Ann Palliat Med 2022;11: 673–83.
- [30] Zhang S, Han D, Tan X, Feng J, Guo Y, Ding Y. Diagnostic accuracy of 18 F-FDG and 11 C-PIB-PET for prediction of short-term conversion to Alzheimer's disease in subjects with mild cognitive impairment. Int J Clin Pract 2012;66:185–98.
- [31] Parikh NS, Kamel H, Zhang C, Gupta A, Cohen DE, de Leon MJ, et al. Association of liver fibrosis with cognitive test performance and brain imaging parameters in the UK Biobank study. Alzheimers Dement 2023;19:1518–28.
- [32] Weinstein G, Schonmann Y, Yeshua H, Zelber-Sagi S. The association between liver fibrosis score and incident dementia: a nationwide retrospective cohort study. Alzheimers Dement 2024;20:5385–97.
- [33] Zargar S, Wani TA. Protective role of quercetin in carbon tetrachloride induced toxicity in rat brain: biochemical, spectrophotometric assays and computational approach. Molecules 2021:26.
- [34] Smyth HF, Smyth HF. Safe practices in the industrial use of carbon tetrachloride. J Am Med Assoc 1936;107:1683–7.
- [35] Sakata T, Watanabe A, Hobara N, Nagashima H. Chronic liver injury in rats by carbon tetrachloride inhalation. Bull Environ Contam Toxicol 1987;38:959–61.
- [36] Bengtsson F, Bugge M, Vagianos C, Jeppsson B, Nobin A. Brain serotonin metabolism and behavior in rats with carbon tetrachloride-induced liver cirrhosis. Res Exp Med (Berl) 1987;187:429–38.
- [37] Thackeray JT, Bankstahl JP, Bengel FM. Impact of image-derived input function and fit time intervals on Patlak quantification of myocardial glucose uptake in mice. J Nucl Med 2015;56:1615–21.
- [38] Zachhuber L, Filip T, Mozayani B, Löbsch M, Scheiner S, Vician P, et al. Characterization of a syngeneic orthotopic model of cholangiocarcinoma by [(18) F]FDG-PET/MRI. Cancers (Basel) 2024;16.
- [39] Fueger BJ, Czernin J, Hildebrandt I, Tran C, Halpern BS, Stout D, et al. Impact of animal handling on the results of 18F-FDG PET studies in mice. J Nucl Med 2006; 47:999–1006.
- [40] Bertoglio D, Deleye S, Miranda A, Stroobants S, Staelens S, Verhaeghe J. Estimation of the net influx rate K(i) and the cerebral metabolic rate of glucose MR(glc) using a single static [(18)F]FDG PET scan in rats. Neuroimage 2021;233:117961.
- [41] Rey-Bretal D, Garcia-Varela L, Gomez-Lado N, Moscoso A, Pineiro-Fiel M, Diaz-Platas L, et al. Quantitative brain [(18)F]FDG PET beyond normal blood glucose levels. Neuroimage 2024;300:120873.
- [42] Prando S, Carneiro CG, Robilotta CC, Sapienza MT. Comparison of different quantification methods for 18F-fluorodeoxyglucose-positron emission tomography studies in rat brains. Clinics (Sao Paulo) 2019;74:e1273.
- [43] Wong KP, Sha W, Zhang X, Huang SC. Effects of administration route, dietary condition, and blood glucose level on kinetics and uptake of 18F-FDG in mice. J Nucl Med 2011;52:800–7.